

Article

Experimental Study on the Oxidation Reaction of Coal-Pyrite and Mineral-Pyrite with the Participation of Fe(III) and Bacteria under Acidic Conditions

Mengya Ma ^{1,2}, Wenfeng Wang ^{1,2,*}, Kun Zhang ³  and Zhixiang Shi ^{1,2,4}

¹ Key Laboratory of Coalbed Methane Resource and Reservoir Formation Process, China University of Mining and Technology, Ministry of Education, Xuzhou 221116, China; mengya-ma@cumt.edu.cn (M.M.); shizhixiang@hebeu.edu.cn (Z.S.)

² School of Resources and Geosciences, China University of Mining and Technology, Xuzhou 221116, China

³ State Key Laboratory of Mining Response and Disaster Prevention and Control in Deep Coal Mines, Anhui University of Science & Technology, Huainan 232001, China; kzhang@aust.edu.cn

⁴ Analysis and Testing Laboratory Center, HUE, Hebei University of Engineering, Handan 056038, China

* Correspondence: wangwenfeng@cumt.edu.cn

Abstract: As one of the crucial factors contributing to coal spontaneous combustion, the oxidation of pyrite is a complex process involving multiple reactions, particularly in the presence of oxidants (Fe^{3+} and O_2) and bacteria. However, experimental results based on mineral-pyrite are not entirely applicable to coal-pyrite due to their differences in formation environments and compositions. This study selected two types of coal-pyrite and one type of mineral-pyrite as research to conduct oxidation experiments with the participation of oxidant (Fe^{3+}) and bacteria (*Acidithiobacillus ferrooxidans*), respectively, to obtain the following conclusions. Under natural conditions, the chemical oxidation rate of pyrite is slow, but the addition of oxidant Fe^{3+} and bacteria can significantly accelerate the oxidation rate. The promotion effect of oxidant Fe^{3+} on the oxidation reaction is stronger than that of bacteria. Under the same conditions, the oxidation rate of coal-pyrite samples is slightly higher than that of mineral-pyrite, due to the relatively higher impurities content, poorer crystal structure, and humic acid in the coal seams. Additionally, different compositions of coal-pyrite samples can lead to various oxidation degrees under different conditions. Therefore, the oxidation process and mechanism of pyrite in coal seams are complex and affected by many factors, which need further study to prevent coal spontaneous combustion accurately and effectively.

Keywords: coal-pyrite; mineral-pyrite; oxidation reaction; oxidant Fe(III); bacterial oxidation



Citation: Ma, M.; Wang, W.; Zhang, K.; Shi, Z. Experimental Study on the Oxidation Reaction of Coal-Pyrite and Mineral-Pyrite with the Participation of Fe(III) and Bacteria under Acidic Conditions. *Energies* **2023**, *16*, 3588. <https://doi.org/10.3390/en16083588>

Academic Editor: Nikolaos Koukoulas

Received: 8 April 2023
Revised: 18 April 2023
Accepted: 19 April 2023
Published: 21 April 2023



Copyright: © 2023 by the authors. Licensee MDPI, Basel, Switzerland. This article is an open access article distributed under the terms and conditions of the Creative Commons Attribution (CC BY) license (<https://creativecommons.org/licenses/by/4.0/>).

1. Introduction

Coal spontaneous combustion is one of the major disasters in coal mining and storage, which can not only burn up coal resources and cause huge economic losses but also produce harmful gases and seriously pollute the environment [1,2]. It mostly occurs in areas of coal accumulation and air leakage and is affected by the accumulation environment (climate, air connectivity, moisture content) and coal properties (carbonization degree, particle size, pyrite content), etc. [3,4]. Among them, pyrite oxidation is one of the main factors contributing to coal spontaneous combustion [3].

As the most widely distributed sulfide mineral in the crustal [5], pyrite is usually found in coal seams in various forms, such as nodular, lenticular, layered, fissure filling, and aggregated massive [6]. Pyrite has the characteristic of self-thermal oxidation, producing ferric sulfate and ferrous sulfate, which makes the coal porosity and increases the contact area with oxygen. These oxidation decomposition products are more oxygen-absorbing than coal and can transfer the adsorbed oxygen to coal particles, causing coal oxidation [7]. Moreover, pyrite has a smaller specific heat capacity, and its temperature increment is three

times larger than that of coal when absorbing the same amount of heat, which accelerates the heating of the coal seam [5,7].

Pyrite can be dissolved and oxidized simultaneously in an acidic solution. The initial step is the adsorption of H₂O and O₂ on the surface of pyrite, which is a prerequisite for the oxidation reaction to occur [8]. Then, Fe²⁺ in the mineral lattice can be dissolved and oxidized to Fe³⁺, and the oxidation intermediates of the sulfur element are further oxidized to SO₄²⁻. Besides, SO₄²⁻ is also the main anion in acid mine drainage (AMD) [9], which can enhance the mobility of some heavy metals and enter the stratum and pollute the environment with the flow of AMD [10]. However, it is important to note that the oxidation reaction of pyrite is relatively slow, especially the oxidation of Fe²⁺ to Fe³⁺, which is also a decisive factor influencing the oxidation rate of pyrite [11]. Several factors influence the oxidation rate of pyrite, including oxidant (Fe³⁺ or O₂), pH, redox potential (E_h), etc. [12].

Under the condition that the solution pH is smaller than 3.0, Fe³⁺ is the dominant oxidant of pyrite and the pyrite oxidation rate initiated by Fe³⁺ is 3–4 orders of magnitude higher than that caused by O₂ [13]. Isotope labeling experiments have demonstrated that the oxygen atoms in the oxidation product of SO₄²⁻ come from H₂O rather than O₂ [14,15]. The oxidation rate of Fe²⁺ in the reaction system is positively correlated with O₂ concentration but negatively correlated with pH value. The increase in pH value will transform Fe³⁺ into Fe(OH)₃, which covers the surface of pyrite to inhibit further oxidation [16]. Besides, Boon et al. [17] found that pyrite is challenging to oxidize when the E_h of the reaction system is below 0.30 V. Sun et al. [18] suggested that the pyrite oxidation rate increases linearly with the increase of E_h between 0.70 V and 0.90 V.

In addition, some bacteria can also participate in the oxidation process of pyrite in coal seams and acid mine water. These bacteria, such as the iron-and-sulfur-oxidizing bacteria *Acidithiobacillus ferrooxidans*, *Acidithiobacillus ferridurans*, and *Acidithiobacillus ferrovarans*; the sulfur-oxidizing bacteria *Acidithiobacillus caldus*, *Acidithiobacillus thiooxidans*, and *Acidithiobacillus albertensis* [19]; and the iron-oxidizing bacteria *Leptospirillum ferrooxidans*, etc., can adsorb on the mineral surface or dissociate in the reaction system, and then secrete various compounds to accelerate the oxidation of iron, sulfur, and other inorganic components [20]. The pyrite oxidation rate by microorganisms is several to even hundreds of times higher than pure chemical oxidation [21], and forms secondary minerals and elements through different oxidation pathways from purely chemical reaction processes [22]. Among them, *Acidithiobacillus ferrooxidans* is considered the most important and representative microorganism in the coal mine acidic environment [23].

In summary, the oxidation process of pyrite is very complex with the participation of oxidants (Fe³⁺ and O₂) and bacteria in the coal seams. However, most of the previous studies have used mineral-pyrite for simulation experiments of pyrite oxidation [5,11,14,24]. There are some differences in the formation environments and compositions between coal pyrite and mineral pyrite, which may lead to incomplete applicability of experimental results based on mineral-pyrite to coal-pyrite. Therefore, this study selected two types of coal-pyrite and one type of mineral pyrite as the research objects and carried out the oxidation experiments with the participation of oxidant (Fe³⁺) and bacteria (*Acidithiobacillus ferrooxidans*), respectively. The difference in the reaction process between coal pyrite and mineral pyrite and the influencing factors were analyzed to help understand the oxidation characteristics of pyrite in coal seams and prevent coal spontaneous combustion.

2. Experiments and Methods

2.1. Sample Information and Preparation

The coal-pyrite samples used in this study were sampled from the coal seam at the Xiongxin Coalmine and Jiashun Coalmine in the Xingyi coalfield, Guizhou province, China, as shown in Figure 1. The coal seams belong to the Upper Permian coal-bearing series and are of the coastal tidal flat-lagoon sedimentary facies [25,26].

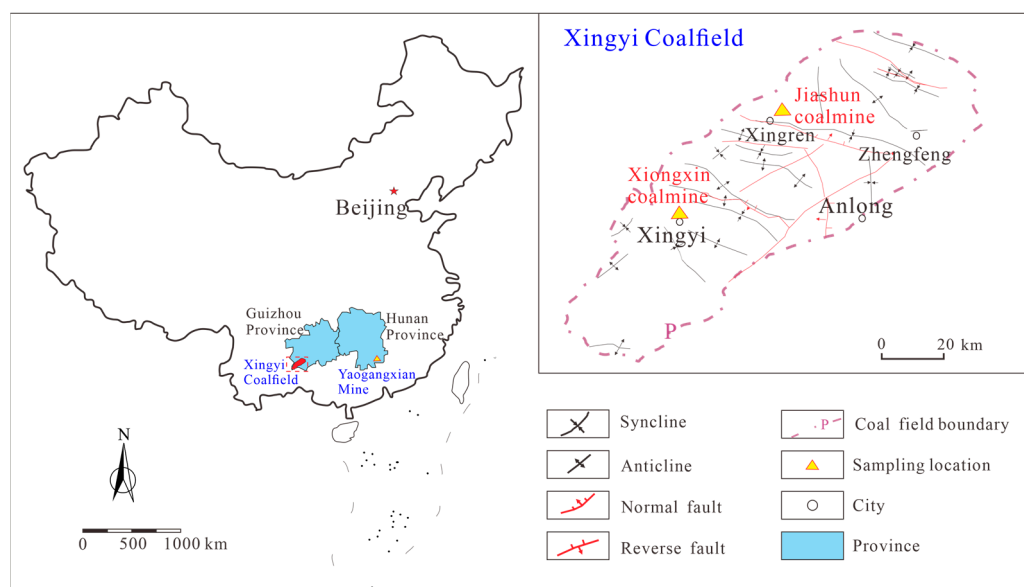


Figure 1. Sampling location of coal-pyrite and mineral-pyrite.

The coal seams were formed in tidal flats adjacent to deltas, and they have a higher sulfur content due to the influence of river and ocean tides [25,26]. The sulfur content of the coal samples is shown in Table 1. According to the China national standard (GB/T 15224.2-2021), the total sulfur of the two coal samples is higher than 3%, which categorizes them as high-sulfur coal. Pyrite is the main form of sulfur in these coal samples, accounting for 68.76% and 89.06%, respectively.

Table 1. Sulfur content in coal samples, wt%.

Coal Mine	Sample ID	$S_{p,d}$			$S_{o,d}$			$S_{s,d}$			Classification
		$S_{t,d}$	S_0	P	S_0	S_0	P	S_0	P		
Jiashun	C1	5.7	3.9	68.8	1.7	29.0	0.1	2.3	High sulfur		
Xiongxin	C2	5.3	4.7	89.1	0.5	9.6	0.07	1.3	($S_{t,d} > 3.0$)		

Note: $S_{t,d}$ is the total sulfur, %; $S_{p,d}$ is the pyritic sulfur, %; $S_{o,d}$ is the organic sulfur, %; $S_{s,d}$ is the sulfate sulfur, %; S_0 is the content of sulfur in the coal, %; and P is the proportion of total sulfur, %.

The coal-pyrite samples need to be screened and extracted from the coal body to obtain the coal-pyrite samples. The coal body was crushed to find the pyrite enrichment profile and site. The pyrite particles were carefully picked out and any impurities were scraped out using tweezers. In addition, a high-purity mineral-pyrite sample collected from the Yaogangxian metal mine in Hunan Province, China, was used as experimental control in this study, which is close to the Guizhou Province and contains pyrite veins with good ore-forming conditions (Figure 1). The sulfur isotopes analysis results of different sulfides in Yaogangxian metal mine show that the source of sulfur in the deposit is single and mainly from magma [27]. Both the coal-pyrite and mineral-pyrite samples were then crushed to the same size (75 μm) to minimize the size effect of the reaction [28]. Subsequently, the samples underwent ultrasonic treatment using deionized water, cleaned with anhydrous ethanol, vacuum dried at 50 °C for 24 h, and were sealed to prevent oxidation.

2.2. Experimental Setup

2.2.1. Oxidation Reaction with Fe^{3+}

To simulate the acidic mine water environment in coal seams, the experimental conditions of the pyrite oxidation reaction are set as pH of 2.0 and temperature of 25.0 °C. Firstly, an experimental solution with 6 mmol/L of Fe^{3+} was prepared using ferric chloride hexahydrate ($\text{FeCl}_3 \cdot 6\text{H}_2\text{O}$) and ultra-pure water. The pH of the solution was adjusted to 2.0

by adding sodium chloride (HCl, with a concentration of 0.5 mol/L) and sodium hydroxide (NaOH, with a concentration of 0.1 mol/L). Then, the solution was injected into a 900 mL reaction container and placed on a magnetic agitator, with corresponding measuring instruments (conductivity instrument, pH meter, and thermometer) connected inside the container. When the solution temperature reached 25.0 °C, the prepared pyrite mineral particles (2.000 ± 0.002 g) were poured into the reaction container and the rotational speed was set at 700 r/min to make the pyrite particles float. The oxidation experiment lasted for 120 min, collected a reaction solution of 5 mL every 30 min, and recorded the measuring date during each collection.

2.2.2. Oxidation Reaction with Bacteria

The *Acidithiobacillus ferrooxidans* (type 23270, from American Type Culture Collection (ATCC)) was selected for the oxidation experiment of pyrite with bacteria. Firstly, a Fe-free 9 K medium of 200 mL was injected into a conical bottle, which was then sterilized at a high temperature and inoculated with a 10% bacterial solution of 20 mL. The bacteria were activated and cultured for three days at a temperature of 30 °C.

To perform the oxidation experiments on pyrite minerals using bacterial leaching, it was necessary to account for the clustering of the bacteria. Firstly, the glass fiber was filled at the bottom of the connected glass tube with an inner diameter of 50 mm and a height of 500 mm. Then 20 g of reagent-grade quartz sand with a particle size of 0.5–1 mm was spread on the glass fiber layer, followed by a mixture of 30 g of quartz sand and 5 g of the prepared pyrite. Next, a 500 mL solution with a pH of 2 was prepared using ultra-pure water and dilute sulfuric acid, and added 10 mL of the activated bacteria solution to it. This solution was proportioned to leach the pyrite sample circularly to prevent bacteria clustering. The leaching experiment lasted for 40 days, and 5 mL of the solution was quantitatively extracted every 5 days for component testing. At the same time, another leaching experiment of the acid solution without bacteria was carried out on mineral-pyrite, as a blank control.

2.3. Analysis Method

2.3.1. Morphology Observation

The morphology and composition of pyrite samples were observed and measured using the FEI Quanta™ 250 scanning electron microscope-energy dispersive spectroscopy (SEM-EDS) at the Advanced Analysis and Computation Center (AACC) of China University of Mining & Technology (CUMT). And the flat and uniform regions on the surface of the pyrites were selected for the EDS analysis. The SEM-EDS was operated in high vacuum mode with a working distance of 14–20 mm, a beam voltage of 30 kV, an aperture of 6 µm, and a spot size of 3.5–5.0 µm.

2.3.2. Mineral Content and Forms of Sulfur

A D8 Advance X-ray diffractometer (XRD) was used to analyze the mineral compositions of the pyrite samples at the AACC of CUMT, with a Cu X-ray source at 40 kV and 30 mA. The tested angle ranged from approximately 3° to 70° and the diffractograms were analyzed by the Jade 6.5 software. Besides, the chemical valence state and relative content of pyrite samples were analyzed using an Escalab 250Xi X-ray photoelectron spectroscopy (XPS). The acquisition parameters of XPS survey scans: the acquisition time is 128 s; the electron gun source type is Al K α , the beam spot is 650 kbps; the step size is 1.0 eV; the energy step number is 1361.

2.3.3. Ion Content in the Solution

The ion content of the oxidation reaction solution was measured after filtration. A Dionex-500 ion chromatograph was used to test the content of SO_4^{2-} produced by the oxidation of pyrite according to the China national standard (GBT5750.5-2006) at the AACC

of CUMT. And the contents of Fe^{2+} and Fe^{3+} were analyzed using a 721-type spectrometer according to the Geological and Mineral Industry Standards of China (DZ/T 0064.23-2021).

3. Experimental Results

3.1. Occurrence and Structure of Pyrite in Coal

3.1.1. Sample Morphology

The macroscopic morphology of mineral-pyrite and coal-pyrite samples were shown in Figure 2. The mineral pyrite presents a regular cubic and pentagonal dodecahedral crystalline shape, characterized by a light brass-yellow hue and high purity, besides some fractured granular morphologies. The original forms of coal-pyrite samples in the coal body comprise aggregated massive pyrite and layered pyrite. Coal-pyrite 1 (C1) is yellow-black and composed of medium-coarse equiaxed crystal grains, while coal-pyrite 2 (C2) is a copper-yellow color, dense layered, with a fine-microcrystalline structure.

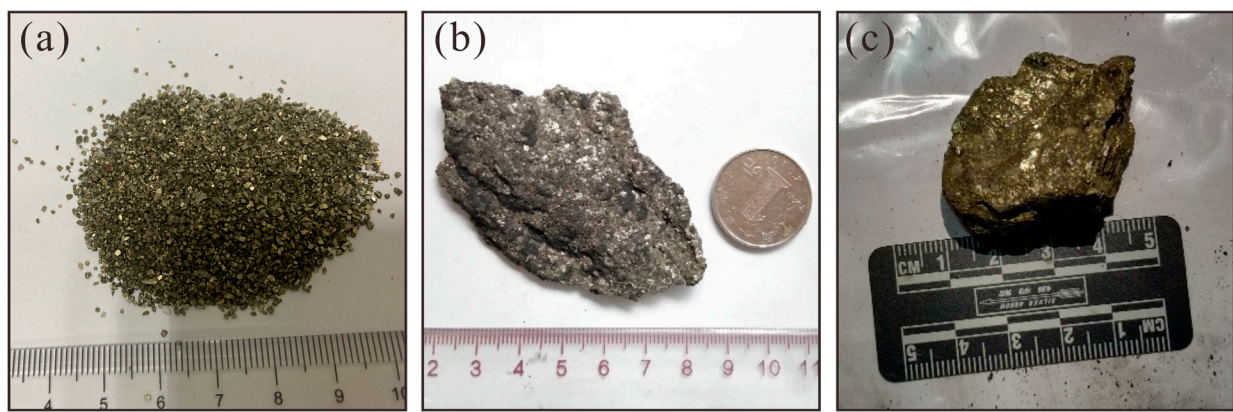


Figure 2. Macromorphology of pyrite: (a) is the mineral-pyrite (M1); (b) is the coal-pyrite from Jiashun coal mine (C1); (c) is the coal-pyrite from Xiongxin coal mine (C2).

The double pycnometer method was utilized to determine the densities of pyrite samples, showing that C1 and C2 possess densities of 3.56 g/cm^3 and 3.63 g/cm^3 , respectively, while mineral pyrite displays a density of 4.92 g/cm^3 . Additionally, the XRD analysis results showed typical diffraction peaks of pyrite minerals in Figure 3, and there are rare diffraction peaks of impurity minerals. It means that the selected pyrite samples possess higher purity and are suitable for the study.

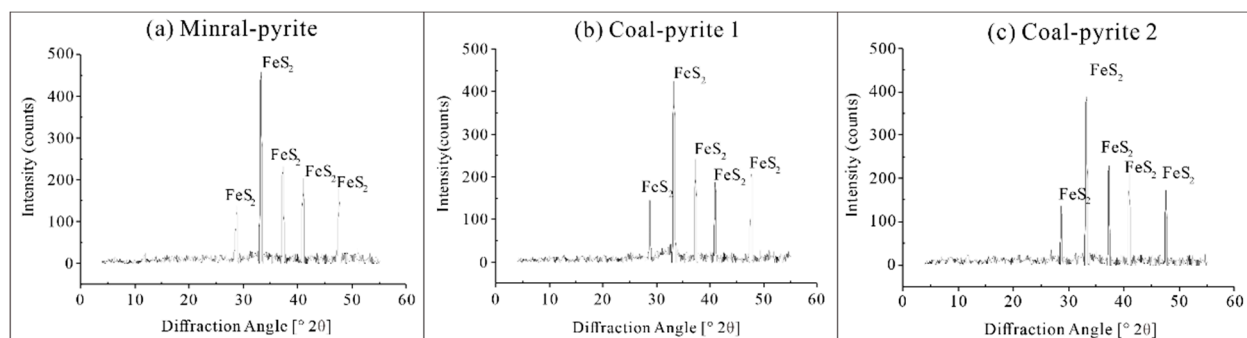


Figure 3. XRD patterns of coal-pyrite and mineral pyrite samples: (a) is the mineral-pyrite (M1); (b) is the coal-pyrite from Jiashun coal mine (C1); (c) is the coal-pyrite from Xiongxin coal mine (C2).

3.1.2. Microscopic Morphology and Composition

The microscopic morphology and composition of pyrite in the coal body were observed and shown in Figure 4 using the SEM-EDS method. These pyrites manifest different shapes, which can be divided into framboidal, fissure-filled, aggregated massive, euhedral crystalline, caviar-like, fine-grained agglomerated pyrites.

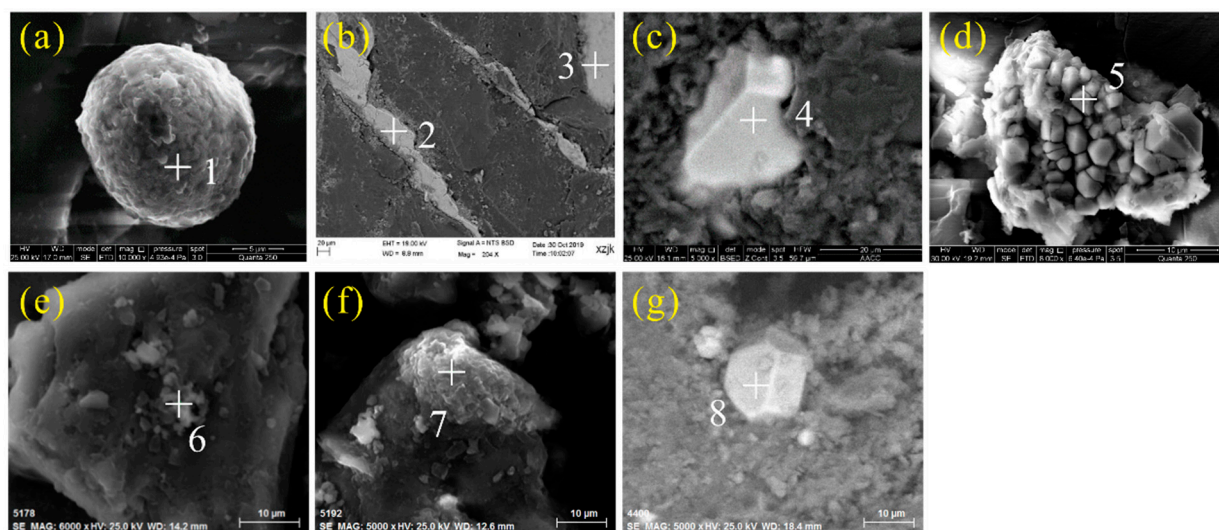


Figure 4. Occurrence forms of pyrite in coal samples: (a) is the framboidal pyrite (site 1); (b) is the fissure-filled (site 2) and aggregated massive pyrite (site 3); (c) is the euhedral crystalline pyrite (site 4); (d) is the caviar-like pyrite (site 5); (e) is the Fine-grained agglomerated pyrite (site 6); (f) is the aggregated massive pyrite (site 7); (g) is the euhedral crystalline pyrite (site 8).

Among them, framboidal pyrites are aggregates of pyrite spheres (Figure 4a) that commonly occur in groups. Filled pyrite is the most prevalent type observed in coals and typically appears in banded (Figure 4b), dendritic, or reticulated patterns. The surface of the agglomerated massive pyrite presents pores and contains organic matter or minerals (Figure 4b), and some are formed by the bonding of fine-grained pyrite particles (Figure 4f). The intact crystal facets of euhedral crystalline pyrites exhibit triangular, square, rhombic, pentagonal, hexagonal, etc. (Figure 4c,g), and are often associated with clay minerals. Caviar-like pyrite has a crystal shape that is densely piled up in groups (Figure 4d) or intermittently distributed along layers in a beaded form. The shape of fine-grained agglomerated pyrite (Figure 4e) appears irregular with uneven edges, semi-colloidal, having a porous surface, and is filled with clay minerals.

The fresh pyrite section displays strong chemical activity and is susceptible to oxidation. Pyrite in coal bodies can be mixed with clay minerals and organic matter, which further affects its properties. The element contents on the pyrite surface were tested by the EDS method, as shown in Table 2. Except for euhedral crystalline and caviar-like pyrite, impurity elements such as carbon and silicon elements were observed in other forms of pyrite. Notably, framboidal, fine-grained agglomerated, and aggregated massive pyrites have a high content of oxygen element, indicating that these pyrites may have been oxidized or mixed with clay minerals.

Table 2. Element content on the coal-pyrite samples/mole fraction %.

Sample ID	Test Site	Morphology	Element Proportion %						N(S)/N(Fe)
			O	S	Fe	Al	Si	C	
C1	1	Framboidal	45.6	23.2	21.7	0.63	0.55		1.07
	2	Fissure-filled	7.3	30.0	16.2			46.5	1.85
	3	Aggregated massive		53.2	38.2	4.5	4.1		1.39
	4	Euhedral crystalline		66.6	33.4				1.99
	5	Caviar-like		53.9	46.1				1.17
C2	6	Fine-grained agglomerated	39.0	30.6	27.9	1.21	1.04	0.25	1.10
	7	Aggregated massive	29.8	21.4	13.9	0.21	0.17	34.5	1.54
	8	Euhedral crystalline	13.1	55.1	30.1	0.81	0.79		1.83

Note: N(S)/N(Fe) is the number ratio of sulfur atoms to iron atoms.

The atomic ratio of sulfur to iron (N(S)/N(Fe)) in pyrite is an indicator of the lattice filling saturation, and lower values suggest more defects in the crystal and greater chemical

reactivity of the pyrite samples. As shown in Table 2, except for euhedral crystalline and fissure-filled pyrite, other forms of pyrite generally exhibit low ratio values, especially fine-grained agglomerated and framboidal pyrite. Similarly, the framboidal pyrite found in the Carboniferous coal-bearing rocks from the Czech part of the Upper Silesian Coal basin also showed a low N(S)/N(Fe) value of 1.02 [29]. Euhedral crystalline pyrite usually forms in the early diagenesis stage, and the fissure-filled pyrite results from hydrothermal fluid precipitation infiltrated into fractures during the epigenetic stage. Both of them form under sufficient time and material supply conditions. However, other forms of pyrite are relatively depleted in sulfur and mixed with organic matter and other minerals in coal seams, leading to their incomplete crystal forms (Figure 4).

The presence of inorganic sulfur and organic sulfur in pyrite samples was analyzed and shown in Figure 5 through the XPS method. Table 3 quantitatively analyzes each component and demonstrates that the proportion of pyrite sulfur amounts to over 76% in these samples. Sulphoxides and thiophenes are the main forms of organic sulfur, and the content of organic sulfur in coal-pyrite is higher than that in mineral-pyrite, indicating a close association between coal-pyrite and organic matter. Besides, the sulfate contents of coal-pyrite samples are higher than that of the mineral-pyrite sample.

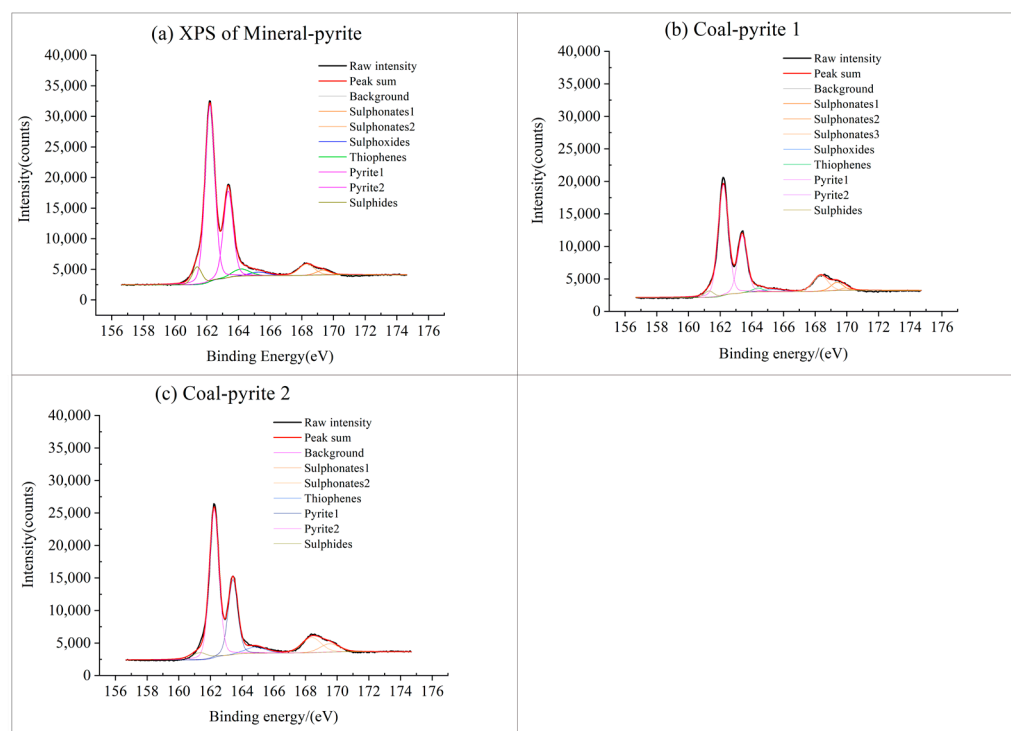


Figure 5. Sulfur types in pyrite samples based on XPS: (a) is the mineral-pyrite (M1); (b) is the coal-pyrite 1 (C1); (c) is the coal-pyrite 2 (C2).

Table 3. Statistics of sulfur content and types based on XPS%.

Sample	Sulfate Sulfur (S _{s,d})	Sulphoxides	Organic Sulfur (S _{o,d}) Thiophenes	Total	Pyrite Sulfur (S _{p,d})	Other Sulfides
M1	2.41	1.16	1.97	3.13	93.08	1.37
C1	14.90	0.00	4.61	4.61	76.90	3.59
C2	16.54	2.09	1.84	3.93	76.71	2.82

3.2. Experimental Results of Pyrite Oxidation

3.2.1. Pyrite Oxidation with Fe³⁺

In the inorganic oxidation experiment of pyrite, Fe³⁺ was used as the oxidant. Figure 6 illustrates the changes in pH value and the concentration of each component (Fe³⁺, Fe²⁺,

and SO_4^{2-}) in the solution during the reaction process. As the reaction progressed, the pH value and the content of Fe^{3+} concentration gradually decreased (Figure 6a,b), indicating that pyrite oxidation involves acid production and oxidant consumption. Moreover, the content of Fe^{2+} and SO_4^{2-} as oxidation products also increased (Figure 6c,d). In the initial stage of the reaction (0–60 min), the content of each component changes rapidly and then tends to become stable.

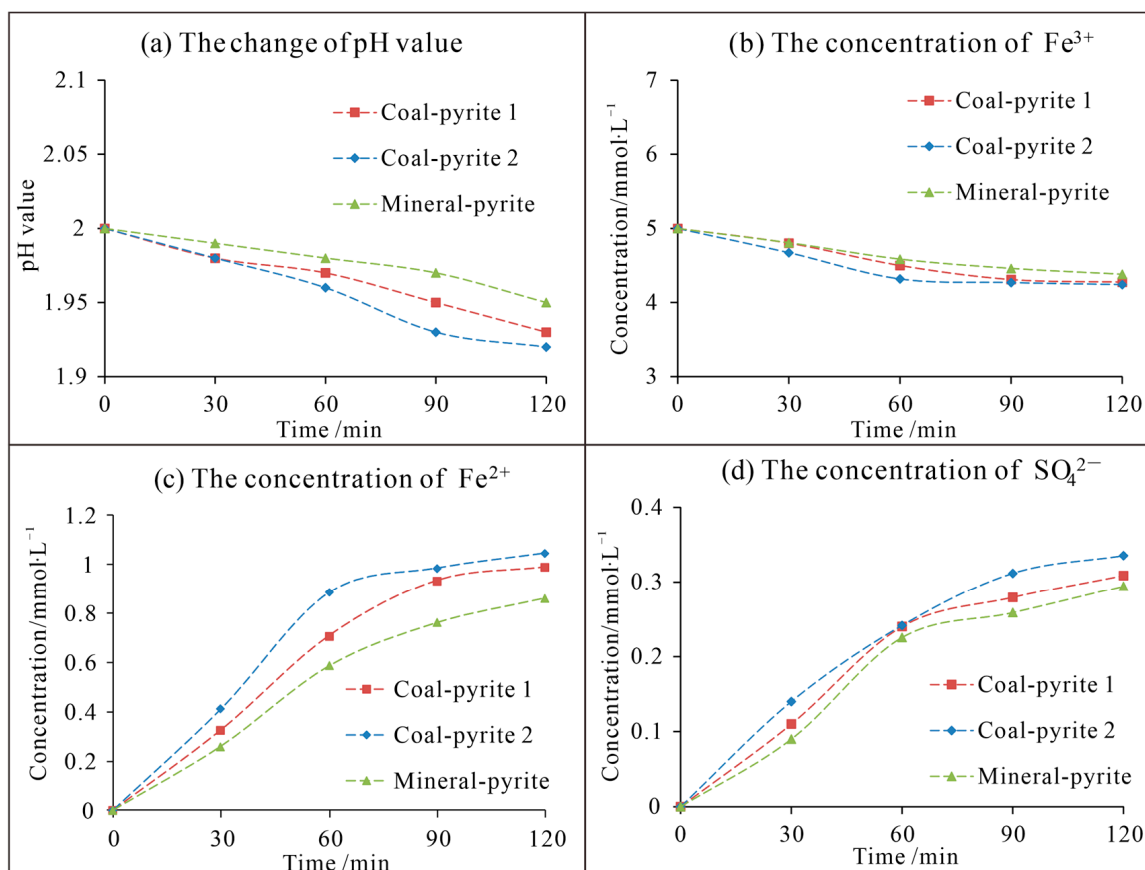


Figure 6. The change of pH value and component concentration in reaction solution with Fe^{3+} : (a) is the change of pH value; (b) is the change of Fe^{3+} concentration; (c) is the change of Fe^{2+} concentration; (d) is the change of SO_4^{2-} concentration.

The consumption of Fe^{3+} as an oxidant to form Fe^{2+} plays a crucial role in determining the oxidation reaction rate of pyrite. The concentration ratio of Fe^{2+} to Fe^{3+} serves as regarded as the oxidation-reduction couples, and the E_h of this reaction system can be calculated according to the Nernst equation:

$$E_h = E_0 - \frac{RT}{F} \ln \left[\frac{[\text{Fe}^{2+}]}{[\text{Fe}^{3+}]} \right] \quad (1)$$

where, E_0 is the standard electrode potential, $E_0 = 770$ mV, R is Avogadro constant, $8.314 \text{ J} \cdot \text{K}^{-1} \cdot \text{mol}^{-1}$; F is Faraday constant, $96,485.33 \text{ C} \cdot \text{mol}^{-1}$, T is the reaction temperature, 298.15 K .

The higher E_h of oxidant in the reaction system has stronger oxidizability. According to the concentration ratio of Fe^{2+} to Fe^{3+} (Figure 7a), the E_h of the reaction system was calculated and measured, as shown in Figure 7b,c. In the initial reaction stage (0–90 min), the significant increase of Fe^{2+} concentration led to a rapid decrease in E_h value. Subsequently, the E_h value exhibited a slow decreasing trend (Figure 7b). Furthermore, the calculated

E_h values of coal-pyrite samples were slightly lower than that of mineral-pyrite. This is because, in the condition of the same oxidation-reduction couples $[\text{Fe}^{2+}/\text{Fe}^{3+}]$, the fast increased concentration of Fe^{2+} in the reaction system of coal-pyrite samples decreases the calculated E_h values at the 30th minute. In addition, the measured E_h values of each reaction system were higher than their calculated values. This could be attributed to the dissolution of other soluble iron-bearing minerals that can be oxidized more easily at the beginning, which increased the measured E_h value and made it higher than the calculated values. Nonetheless, their impact on the reaction system gradually reduced as the reaction proceeded. The measured E_h values of each pyrite sample were similar in the later stage.

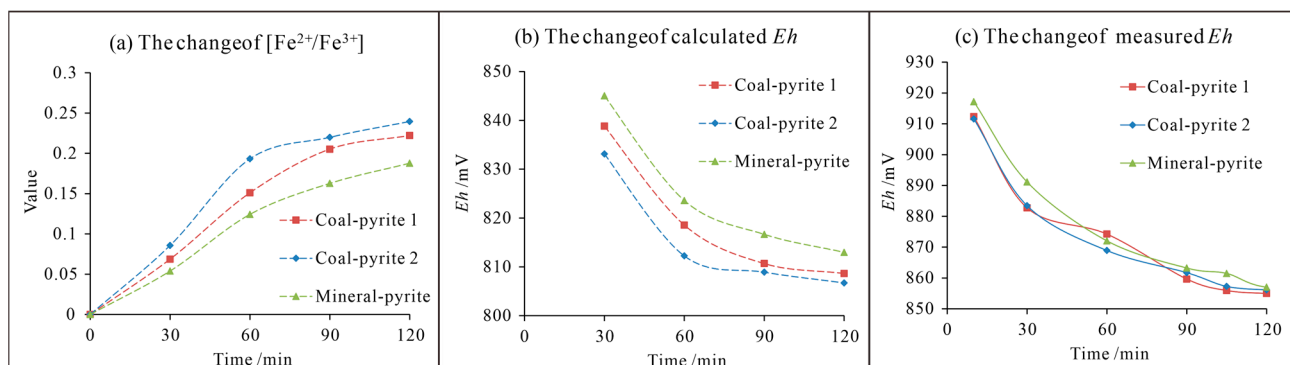


Figure 7. The concentration ratio of Fe^{2+} and Fe^{3+} and the calculated value and test value of E_h : (a) is the concentration ratio of Fe^{2+} to Fe^{3+} ; (b) is the calculated value of E_h ; (c) is the measured value of E_h .

3.2.2. Pyrite Oxidation with Bacteria

Similarly, in the pyrite biological oxidation experiment carried out with *Acidithiobacillus ferrooxidans* under acidic conditions, changes in pH and the concentration of components (Fe^{2+} , Fe^{3+} , and SO_4^{2-}) in the solution were measured and shown in Figure 8. Comparison of the pH and component concentration in the reaction solution of mineral-pyrite (M1) without bacteria revealed that the addition of *Acidithiobacillus ferrooxidans* significantly improves the degree of pyrite oxidation. Moreover, the increase of product (SO_4^{2-}) in the mineral-pyrite (M1) with bacteria was 13-fold higher than that in M1 without bacteria. Due to the relatively small number of microorganisms, the composition in the reaction system of each pyrite sample changed slowly during the initial stage (0–10 days), and then, the rate of change of each ion concentration increased.

In the reaction system of the pyrite-with bacteria, the pH value gradually decreased, while it initially increased and then decreased in the reaction system of M1-without bacteria. This may be related to the consumption of H^+ by the dissolution of pyrite and its impurities, followed by the slow and weak production of H^+ during the pyrite oxidation. The concentration of the redox products (Fe^{2+} and SO_4^{2-}) continually increased throughout the reaction. While the Fe^{3+} content was found to increase initially and then decrease, which might be due to the Fe^{3+} formed in the initial stage participating in the inorganic oxidation reaction of pyrite as an oxidant. Furthermore, the variation range for each component in the coal-pyrite reaction system was slightly higher than that of mineral-pyrite.

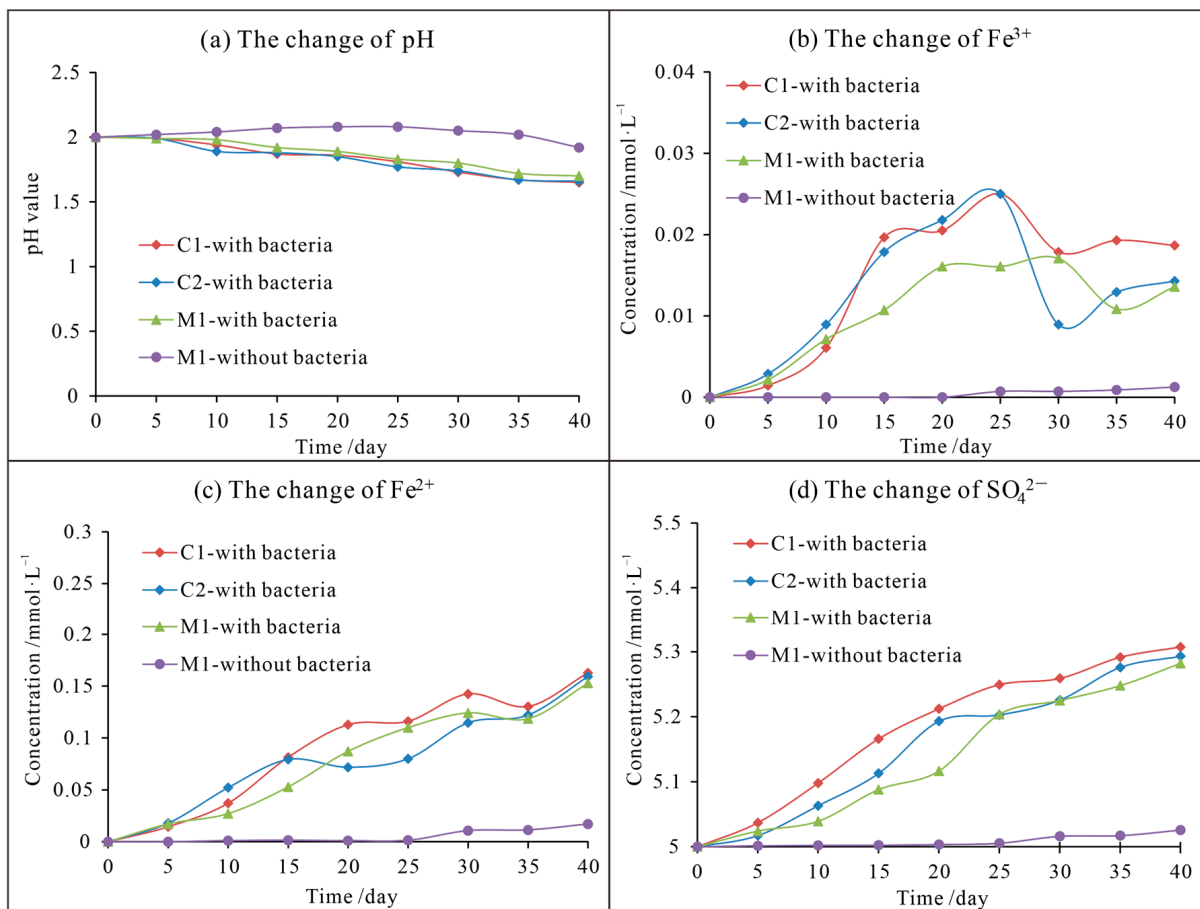


Figure 8. The change of pH value and component concentration in reaction solution with bacteria: (a) is the change of pH value; (b) is the change of Fe³⁺ concentration; (c) is the change of Fe²⁺ concentration; (d) is the change of SO₄²⁻ concentration.

3.2.3. Oxidation Reaction Rate

Based on the experimental conditions, the SO₄²⁻ in the inorganic oxidation reaction system with Fe³⁺ is produced by the oxidation of pyrite. Therefore, the concentration change rate of SO₄²⁻ can be used to represent the pyrite oxidation rate. Similarly, in the biological oxidation reaction system with bacteria, since the addition of sulfuric acid to adjust the pH value, the concentration change rate of iron ions (Fe²⁺ and Fe³⁺) was selected to characterize the pyrite oxidation rate. The atomic ratio of Fe to S in pyrite is 2:1, and the pyrite oxidation rate (*R*) can be expressed as follows:

$$R = -\frac{d[pyrite]}{dt} = \frac{d[SO_4^{2-}]}{2dt} = \frac{d([Fe^{2+}] + [Fe^{3+}])}{dt} \tag{2}$$

where, *[pyrite]*, *[SO₄²⁻]*, *[Fe²⁺]*, and *[Fe³⁺]* are the concentration changes of *pyrite*, SO₄²⁻, Fe²⁺, and Fe³⁺ in the reaction system, respectively; *t* is the reaction time.

The variation trend of oxidation rates of these pyrite samples under Fe³⁺ and bacteria conditions is shown in Figure 9. The oxidation rate of pyrite under the Fe³⁺ condition was significantly higher than that under the bacteria condition. In addition, the oxidation rate decreased gradually with reaction time.

In the M1-without bacteria system, the oxidation rate of pyrite was initially very slow but increased noticeably until the 20th day. However, under the influence of bacteria, the oxidation rate of pyrite increased first and then decreased with reaction time. This means that the initial oxidation rate was slower, and the oxidation rate of pyrite gradually

increased as oxidizing bacteria reproduced. Subsequently, as pyrite was gradually oxidized completely, the oxidation rate of pyrite decreased accordingly.

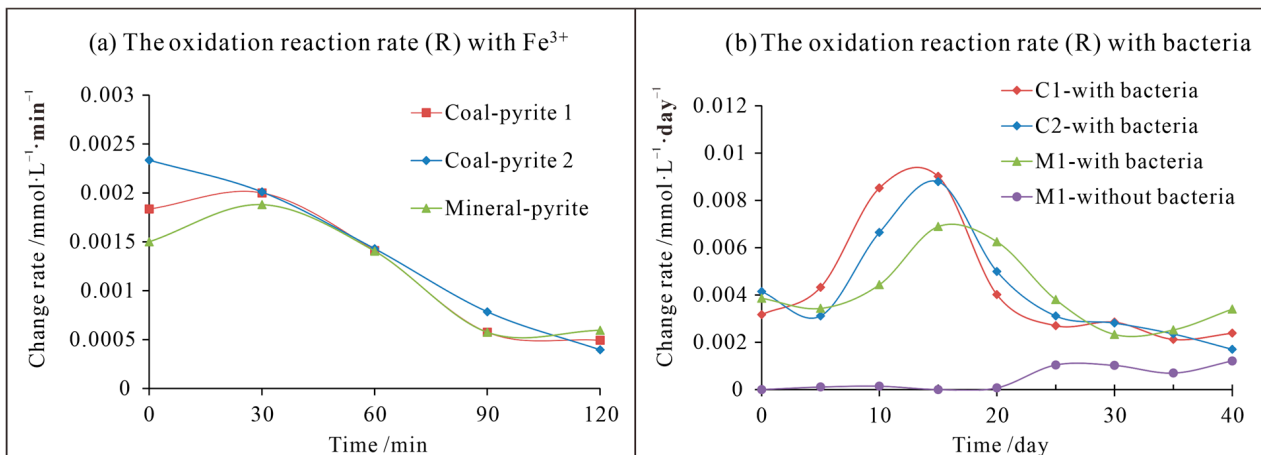


Figure 9. The oxidation rate of pyrite in different conditions of the reactions system: (a) is the pyrite oxidation rate (R) with Fe^{3+} ; (b) is the pyrite oxidation rate (R) with bacteria.

4. Discussion

4.1. Mechanism of the Pyrite Oxidation Reaction

4.1.1. Oxidation Mechanism under the Fe^{3+}

Pyrite contains Fe and S with valences of +2 and −1, respectively, which are both unstable [30]. The active center (Fe^{2+}) on the pyrite surface can continuously adsorb O_2 and H_2O , undergo redox reactions, and release heat [24]. A schematic diagram presented the cyclic oxidation exothermic reaction process of pyrite, as shown in Figure 10.

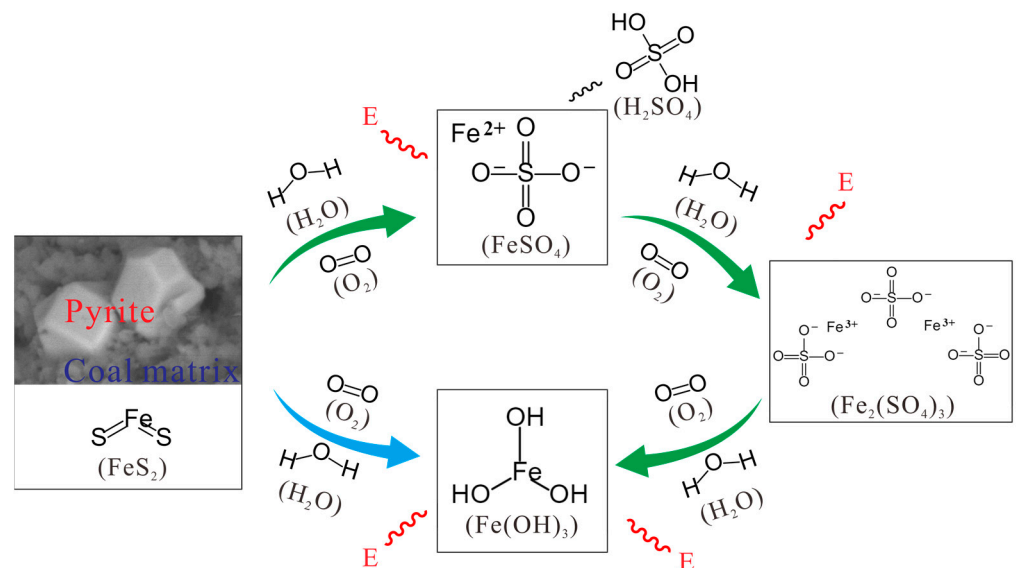
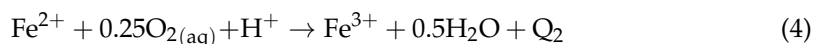


Figure 10. The schematic diagram of the cyclic oxidation exothermic reaction process of pyrite.

The initial step in the oxidation process of pyrite involves the absorption of O_2 and H_2O on its surface, particularly at regions with high surface energy such as lattice defects, corners, and edges of the crystal. This led to the generation of H^+ , Fe^{2+} , and SO_4^{2-} . The chemical reaction formula is as follows:



Under sufficient oxygen condition, FeSO_4 will be further oxidized to form $\text{Fe}_2(\text{SO}_4)_3$ according to the following reaction:



The chemical equilibrium equation for this reaction is as follows:

$$\lg[\text{Fe}^{2+}] = \lg[\text{Fe}^{3+}] - 0.25\lg[\text{O}_2] + \text{pH} - \lg K \quad (5)$$

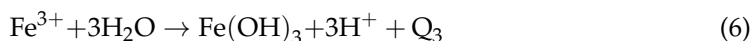
In this experiment, the reaction solution is under sealed conditions with an initial Fe^{3+} concentration of 6 mmol/L and a pH of 2.0. The saturated concentration of dissolved oxygen is 8.25 mg/L at 25.0 °C. According to the equilibrium parameters of this reaction (Table 4), the concentration of Fe^{2+} that may be oxidized is calculated to be 3.15×10^{-14} mol/L. Previous research has shown that Fe^{2+} concentration dominates the oxidation of pyrite when $\text{pH} < 4$ [31]. Therefore, it can be considered that Fe^{2+} is stable under these experimental conditions.

Table 4. Chemical reaction parameters during the oxidation of pyrite.

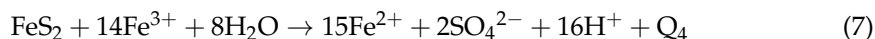
Chemical Equation	Temperature (°C)	ΔH (kJ)	ΔS (J/K)	ΔG (kJ)	K	Lg(K)
Equation (3)	25	−1285.507	−563.038	−1117.637	6.632×10^{195}	195.822
Equation (4)	25	−99.673	−62.924	−80.912	1.502×10^{14}	14.177
Equation (6)	25	96.507	−22.294	103.154	8.441×10^{-19}	−18.074
Equation (7)	25	109.910	317.894	15.130	2.234×10^{-3}	−2.651

Where ΔG is the Gibbs free energy change; ΔH is the enthalpy change; ΔS is the entropy change; K is the reaction equilibrium constant.

The added Fe^{3+} in the experimental solution may be hydrolyzed, as shown in Equation (6):



At the same time, Fe^{3+} in the system will oxidize pyrite as an oxidant, producing a large amount of Fe^{2+} , according to Equation (7), to form an “oxidation-reduction-reoxidation” reaction cycle of pyrite.



In summary, the cyclic oxidation process of pyrite under oxygen-rich conditions can be expressed by Equations (3), (4) and (7), with the final products of Fe^{3+} and SO_4^{2-} . Among them, the reaction rate of Equation (4) is relatively slow and controls the oxidation rate of pyrite.

In addition, according to Table 4, Equations (3) and (4) can occur spontaneously at room temperature ($\Delta G < 0$), and both of them are exothermic reactions ($\Delta H < 0$), particularly Equation (3). The Gibbs free energy change calculation ($\Delta G = \Delta H - T \times \Delta S$) indicates that Equation (7) is only spontaneously carried out at an ambient temperature of 345.74 K (72.59 °C). It means that Equation (7) can easily occur when the continuous occurrence of Equations (3) and (4) results in a temperature increase within the system, leading to the cyclic oxidation exothermic reaction of pyrite.

4.1.2. Oxidation Mechanism under the Bacteria

The pyrite oxidation by bacteria is a combined process including direct contact and indirect contact [32]. In direct contact oxidation, microorganisms adsorb on the mineral surface, dissolve and oxidize pyrite to form Fe^{2+} and SO_4^{2-} directly through the metabolites or biological enzymes [33]. In indirect contact oxidation, microorganisms increase the rate of Fe^{2+} oxidation to Fe^{3+} without directly touching the pyrite surface. The mechanism of the pyrite oxidation by microbial was summarized based on previous research [34–36], which is shown in Figure 11. Firstly, microorganisms grow rapidly by oxidizing Fe^{2+} in the solution,

and the formed Fe^{3+} can further oxidize sulfur on the surface of pyrite, leading to a weak dissolution pit [36,37]. This process lasts for a relatively long time (Figure 11a). For instance, the concentrations of Fe^{3+} and SO_4^{2-} began to increase rapidly on the 10th–15th day in this study (Figure 9b).

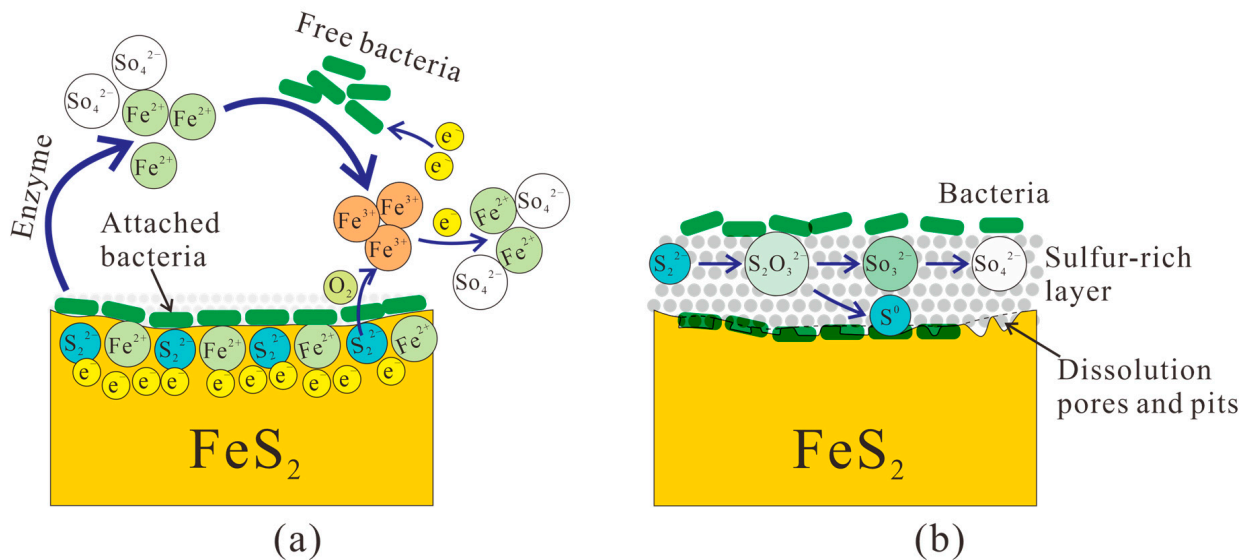
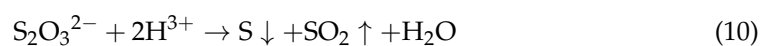
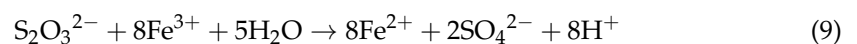


Figure 11. The mechanism of bacterial action on pyrite: (a) is the bacteria involved in pyrite oxidation process; (b) is the sulfur speciation changes on pyrite surface.

Subsequently, microorganisms continuously attached to the pyrite surface and formed microbial films, leading to the appearance of numerous dissolution pits and secondary precipitation appeared on the surface [38]. With the synergistic oxidation and erosion of pyrite by microorganisms and Fe^{3+} , a large number of erosion pits are formed on the surface and develop deep (Figure 11b). However, since the pyrite samples used in this study were crushed into particles, only a part of the pyrite surfaces was observed to be blurred by SEM method, as shown in Figure 12. Energy dispersive (EDS) analysis results showed that the pyrite surface had high contents of oxygen and carbon elements, which may be related to the biological oxidation of pyrite. Previous studies have found two types of dissolution pits formed on the surface of pyrite after being oxidized by microorganisms: cell morphology and mineral morphology [36,37]. The former is formed by microbial metabolism directly eroding the pyrite surface, while the latter is the chemical oxidation product of pyrite by Fe^{3+} and appears in a regular hexagon.

In addition, previous studies [36,39] have shown that during the oxidation process of pyrite by microorganisms, the persulfate ions (S_2^{2-}) are oxidized first to form thiosulfate ($\text{S}_2\text{O}_3^{2-}$), which then be oxidized to form SO_4^{2-} by Fe^{3+} , as shown in Equations (8) and (9). However, under acidic conditions, $\text{S}_2\text{O}_3^{2-}$ can undergo disproportionation to produce native sulfur (S_0) and SO_2 (Equation (10)). The formed SO_2 dissolves in water and is further oxidized to form SO_4^{2-} (Equations (11) and (12)). Therefore, the oxidized surface of pyrite under the action of microorganisms may produce sulfur-rich layers of different forms of sulfur, as shown in Figure 11b. Li et al. [36] detected multiple sulfur-containing components on the pyrite surface using the XPS method after microbial oxidation, such as $\text{S}_2^{2-}/\text{S}^{2-}$, S_n^{2-} , S_0 , $\text{S}_2\text{O}_3^{2-}$, SO_3^{2-} and SO_4^{2-} , etc.



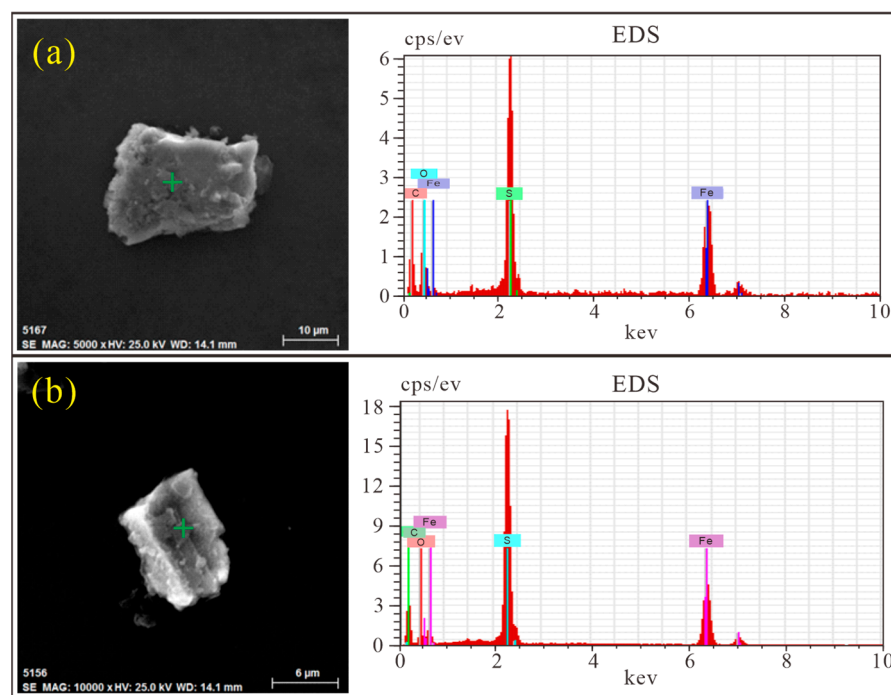


Figure 12. Analysis of pyrite surface after microbial action: (a) is the Coal-pyrite 1; (b) is the Coal-pyrite 2.

4.2. Differences between Coal-Pyrite and Mineral-Pyrite

This study conducted oxidation experiments on mineral-pyrite and coal-pyrite under the addition of Fe^{3+} and microorganisms, respectively. The results showed that under the same conditions, the change in each component in the reaction system of coal-pyrite was higher than that of mineral-pyrite (Figures 6 and 8). Moreover, the oxidation rate of coal-pyrite was also higher than that of mineral-pyrite in the initial reaction (Figure 9). As shown in Figures 2 and 4, coal-pyrite samples displayed high heterogeneity, with different mineral composition and crystal structure compared to mineral-pyrite. In addition, the organic matter in the coal body can also affect the oxidation process of pyrite.

4.2.1. Mineral Impurities

The final products of pyrite oxidation are $\text{Fe}^{2+}/\text{Fe}^{3+}$ and SO_4^{2-} . As mentioned in Section 3.2.3, SO_4^{2-} in the reaction system with Fe^{3+} was produced by the pyrite oxidation, while the iron ions (Fe^{2+} and Fe^{3+}) were formed by the pyrite oxidation in the reaction system with bacteria. After subtracting the ion content change in the original reaction solution, the increase of iron ion and SO_4^{2-} caused by pyrite oxidation under the action of Fe^{3+} and bacteria were calculated respectively, and presented in Table 5. However, the concentration increase of iron ion and SO_4^{2-} did not meet the ratio of 1:2, indicating that there are other mineral impurities involved in the reaction besides pyrite even though these pyrite samples have been purified.

A concentration difference parameter (D) was used to characterize the reaction degree of mineral impurities, defined as the concentration difference between the theoretical increase value and the actual increase value of a certain component:

$$D = [\text{Measured value}] - [\text{Calculated values}] \quad (13)$$

Since the SO_4^{2-} in the Fe^{3+} reaction system only came from pyrite, the theoretical concentration increase value of iron ion was calculated according to the concentration increment of SO_4^{2-} , and then obtained the concentration difference parameter (D_{Fe}) of iron ion. Similarly, calculated the concentration difference parameter (D_{S}) of SO_4^{2-} in the bacterial reaction system. The calculation results were shown in Figure 13.

Table 5. The concentration increase of iron ion and SO_4^{2-} caused by pyrite oxidation, mmol/L.

Reaction Conditions	Reaction Time									
	0 min		30 min		60 min		90 min		120 min	
	Iron Ion	SO_4^{2-}	Iron Ion	SO_4^{2-}	Iron Ion	SO_4^{2-}	Iron Ion	SO_4^{2-}	Iron Ion	SO_4^{2-}
M1- with Fe^{3+}	0	0	0.068	0.09	0.173	0.225	0.224	0.259	0.245	0.294
C1- with Fe^{3+}	0	0	0.128	0.11	0.21	0.24	0.246	0.279	0.266	0.309
C2- with Fe^{3+}	0	0	0.085	0.14	0.205	0.241	0.257	0.312	0.291	0.335
Reaction conditions	Reaction Time									
	0 day		5 day		10 day		15 day		20 day	
	Iron ion	SO_4^{2-}	Iron ion	SO_4^{2-}	Iron ion	SO_4^{2-}	Iron ion	SO_4^{2-}	Iron ion	SO_4^{2-}
M1-without bacteria	0	0	0	0.002	0.001	0.002	0.001	0.002	0.001	0.003
M1-with bacteria	0	0	0.019	0.024	0.034	0.039	0.064	0.088	0.103	0.116
C1-with bacteria	0	0	0.016	0.037	0.043	0.098	0.101	0.166	0.133	0.212
C2-with bacteria	0	0	0.021	0.017	0.031	0.063	0.087	0.113	0.119	0.193
Reaction conditions	Reaction Time									
	25 day		30 day		35 day		40 day			
	Iron ion	SO_4^{2-}	Iron ion	SO_4^{2-}	Iron ion	SO_4^{2-}	Iron ion	SO_4^{2-}		
M1-without bacteria	0.002	0.005	0.011	0.016	0.012	0.017	0.018	0.026		
M1-with bacteria	0.126	0.204	0.141	0.225	0.149	0.248	0.166	0.282		
C1-with bacteria	0.141	0.249	0.160	0.259	0.170	0.291	0.182	0.307		
C2-with bacteria	0.137	0.203	0.150	0.225	0.165	0.276	0.174	0.293		

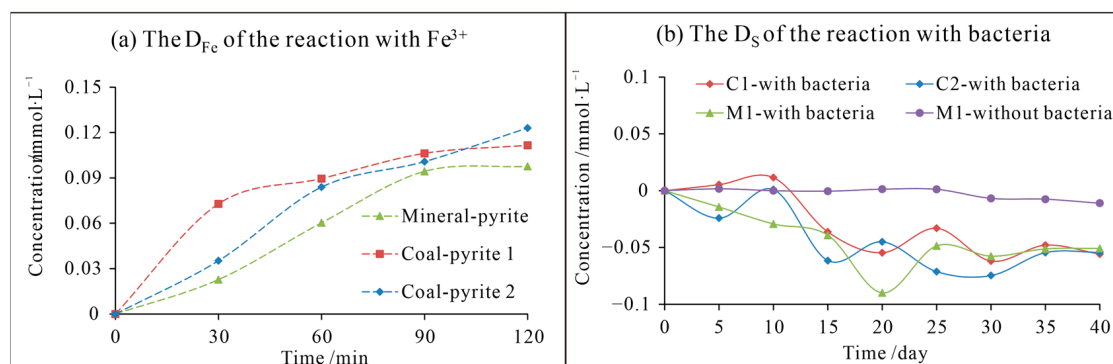


Figure 13. The calculation results of the concentration difference parameters in the two reaction systems: (a) is the concentration difference parameter of iron ion (D_{Fe}); (b) is the concentration difference parameter of SO_4^{2-} (D_{S}).

It can be seen in Figure 13a that the concentration difference parameter of ions ion (D_{Fe}) is a positive value and the measured increase value is slightly higher than the calculated value. This suggests that some iron-containing minerals were dissolved in the reaction system. Except for pyrite, the common iron-containing minerals in coal seams include siderite (FeCO_3), ankerite ($\text{Ca}(\text{Mg}, \text{Fe})(\text{CO}_3)_2$), etc. These minerals are more easily dissolved in acid solutions, resulting in a higher Fe^{2+} concentration increase and reaction rate in the coal-pyrite reaction system than in the mineral-pyrite system in the initial stage (Figures 6c and 9a). At the same time, the pH value of the reaction solution of M1-without bacteria slightly increased in the early stage, as shown in Figure 8a, which also reflected the consumption of H^+ by the dissolution of impurity minerals. Coal-pyrite samples have relatively higher impurity content than mineral-pyrite, and the growth rate of Fe ion content in the early stage is faster (Figure 6c). As the reaction progressed, the D_{Fe} increased slowly, indicating that the influence of mineral impurities on the reaction gradually reduces.

The pyrite oxidation by microorganisms is a relatively complex process (Figure 11). During this process, sulfur in pyrite can be oxidized into various forms, resulting in a

negative value of D_s (Figure 13b) and the relatively deficient content of SO_4^{2-} in the initial stage of the reaction. As the reaction progressed, other forms of sulfur are eventually oxidized to SO_4^{2-} , and the absolute value of D_s decreases. However, the actual increase value of SO_4^{2-} was always smaller than the calculated value, indicating a greater increase of iron ions in the reaction system.

4.2.2. Crystal Structure

The formation process of pyrite involves two evolution modes, direct precipitation and comprehensive genesis [40]. During this process, impurity elements can enter the lattice by lattice substitution and isomorphism. For instance, Co, Ni, and Cu can replace Fe atoms, and As, Se and Te can replace S atoms [41]. Alternatively, impurity elements can enter the crystal gap in the form of mechanical mixtures, such as Au, Ag, Pb, and Zn [42], resulting in crystal defects of pyrite minerals. Murphy et al. [43] confirmed that crystal defects can cause pyrite crystals to break and dissociate easily, and the under-coordinated Fe atoms in the fracture boundary region will react with the surrounding paramagnetic materials, such as O_2 . In the meanwhile, the impurity elements in the lattice can catalyze the oxidation of pyrite. Liu et al. [44] have found that the morphology and distribution of the impurity elements in pyrite crystal can significantly affect the corresponding oxidation activity of pyrite. Due to the differences in genesis and sedimentary environment, there are obvious differences in crystal structure between coal-pyrite and mineral-pyrite. Coal-pyrite samples have lower lattice filling saturation (Table 2), and their densities are also much smaller than mineral-pyrite, indicating that the internal defects of coal pyrite are more noticeable [45] and make it easier to be oxidized (Figure 9).

As mentioned earlier, the oxidation reaction of pyrite occurs on the crystal surface, and a larger contact area between pyrite crystal and $\text{O}_2/\text{H}_2\text{O}$ leads to a faster reaction rate. The complex genesis results in various forms of coal-pyrite (Figure 4). For instance, framboidal and caviar-like pyrite have mineral morphologies similar to spherical or spherical mass, providing much larger specific surface areas than the mineral-pyrite that is dominated by regular cube and pentagonal dodecahedron. Moreover, the lattice filling saturations of these two pyrites are relatively low, with the $N(\text{S})/N(\text{Fe})$ ratios of 1.07 and 1.17, respectively (Table 2), which further improves the oxidation reaction rate. In addition, coal seams commonly contain a significant amount of fine-grained euhedral crystalline pyrite with diameters less than $60\ \mu\text{m}$ [6], which provides a larger specific surface area for the oxidation reaction.

4.2.3. Organic Matter

Compared to mineral-pyrite, the formation of coal-pyrite is more obviously affected by organic matter. Coal seams contain a large number of humic acids that are rich in active groups, such as carboxyl and hydroxyl functional groups [46], which have strong capabilities of adsorption, complexation, and ion exchange [47]. Humic acid has a complicated effect on the oxidation of pyrite. On the one hand, the adsorption of humic acid on the pyrite surface can slow down or even prevent the interface reaction between $\text{Fe}^{3+}/\text{O}_2$ and pyrite [43]. On the other hand, humic acid can promote the production of hydroxyl radical of pyrite and enhance the oxidation ability [48], although some scholars believe that humic acid cannot change the oxidation mechanism of pyrite [49]. Moreover, humic acid and organic matter in the coal seams can provide carbon nutrients for microorganisms, which leads to the proliferation of microbes, and their metabolites and metabolic activities can also destroy the humic acid layer on the pyrite surface [50]. The coal-pyrite samples used in this study have been broken and purified before the oxidation experiment, so the residual humic acid can hardly form a dense barrier layer on the surface. Therefore, it is considered that residual humic acid is beneficial to the oxidation of coal-pyrite in this study.

In addition, coal-pyrite contains a higher content of organic sulfur than mineral-pyrite (Table 3), which mostly exists in the form of sulphoxides and thiophenes. Previous studies have shown that sulfide sulfur can be oxidized to sulfoxide at low temperatures and

further oxidized to form sulfone [51]. The oxidation of organic sulfur by microorganisms promotes the enrichment of sulfur on the mineral surface, but it is difficult to transform into SO_4^{2-} [52]. Therefore, the concentration change of SO_4^{2-} under the bacteria action comes from the oxidation of pyrite (Figure 8d).

In summary, the differences in mineral impurity composition, crystal structure, and organic components between coal-pyrite and mineral-pyrite lead to a high oxidation rate of coal pyrite in this experiment. Besides, probably due to the different compositions and environments, the oxidation rate of the C2 sample is higher than that of the C1 sample in the Fe^{3+} condition, while the C1 sample has a higher oxidation reaction degree than the C2 samples under the action of microorganisms. Therefore, further research is necessary to study the oxidation mechanism of pyrite in coal seams under the influence of multiple factors.

4.3. Inspiration to Prevent Coal Spontaneous Combustion

The oxidation of pyrite plays a crucial role in the occurrence of coal spontaneous combustion [53]. The natural chemical oxidation rate of pyrite is generally slow and uniform, such as the reaction of M1-without bacteria in this study (Figure 9b), but the oxidation rate can be greatly increased under the participation of Fe^{3+} and bacteria conditions. Some studies have shown that the oxidation rate of pyrite in acidic water with microorganisms can be increased by 10^6 times, which is 10–20 times faster than that of the inorganic chemistry reaction under Fe^{3+} condition [54]. Furthermore, the oxidation rate of coal-pyrite is higher than that of mineral-pyrite under the influence of multiple factors.

Therefore, preventing the catalytic effect of Fe^{3+} and bacteria on pyrite oxidation is an important method to avoid coal spontaneous combustion. According to the reaction process of pyrite oxidation and exotherm (Figure 10), the accumulation of moisture, temperature, and heat will form a reaction cycle of “oxidation-reduction-reoxidation” of pyrite. Therefore, it is essential to monitor the temperature and humidity of the coal accumulation environment and ensure that the air remains calm [55]. In addition, the bio-oxidation of pyrite by microorganisms cannot be ignored. Antibiotics and surfactants can be sprayed regularly on tailings and gangue to sterilize and prevent microorganisms from contact with pyrites, such as Triclosan, Kathon (isothiazolinones), and sodium dodecyl sulfate (SDS) [56].

5. Conclusions

In this study, two kinds of coal-pyrite and one kind of mineral-pyrite samples were used to conduct the oxidation experiments under the participation of Fe^{3+} and *thiobacillus ferrooxidans* in acid solutions. Through analyzing the changes in pH and each component in the reaction system, the following conclusions were drawn:

- (1) The natural chemical oxidation rate of pyrite is slow and uniform. The participation of oxidant Fe^{3+} and bacteria can significantly increase the oxidation rate of pyrite, although their action process and mechanism are different. In this study, bacteria had a lower impact on the pyrite oxidation than the oxidant.
- (2) Under the same conditions, the oxidation degree and rate of coal-pyrite samples were slightly higher than those of mineral-pyrite. The relatively higher impurities content and more incomplete crystal structure of coal-pyrite samples can help to improve the oxidation reaction rate. Moreover, the organic matter in coal has a close relationship with coal-pyrite and affects the oxidation process of coal-pyrite.
- (3) Compared to mineral-pyrite, the oxidation process and mechanism of coal-pyrite are more complex and affected by many factors. The various compositions of coal-pyrite samples can also lead to different oxidation processes. It is necessary to carry out an in-depth study to understand the oxidation mechanism of coal-pyrite under the influence of multiple factors and take corresponding measures to prevent coal spontaneous combustion accordingly.

Author Contributions: Methodology, W.W.; Validation, Z.S.; Investigation, Z.S.; Resources, W.W.; Writing—original draft, M.M.; Writing—review & editing, K.Z.; Funding acquisition, W.W. and K.Z. All authors have read and agreed to the published version of the manuscript.

Funding: This research was funded by the National Natural Science Foundation of China (Nos. U1903207, 41972176, 42202200), and the National Key R&D Project of China (No. 2021YFC2902003), the Major Science and Technology Special Project of Xinjiang Uygur Autonomous Region ((No. 2022A03014). The APC was funded by the Science and Technology Basic Work of Science and Technology (No. 2022xjkk1003) and the Major Special Projects of Science and Technology of Anhui Province (No. 202203a07020010).

Data Availability Statement: Data is contained within the article.

Acknowledgments: We would like to thank the anonymous reviewers for their constructive and detailed comments on this manuscript.

Conflicts of Interest: The authors declare no conflict of interest.

References

1. Wen, H.; Wang, H.; Liu, W.; Cheng, X. Comparative study of experimental testing methods for characterization parameters of coal spontaneous combustion. *Fuel* **2020**, *275*, 117880. [[CrossRef](#)]
2. Xia, T.; Zhou, F.; Wang, X.; Zhang, Y.; Li, Y.; Kang, J.; Liu, J. Controlling factors of symbiotic disaster between coal gas and spontaneous combustion in longwall mining gobs. *Fuel* **2016**, *182*, 886–896. [[CrossRef](#)]
3. Ding, C.; Li, Z.; Wang, J.; Duanmu, P.; Lu, B.; Gao, D. Experimental research on the spontaneous combustion of coal with different metamorphic degrees induced by pyrite and its oxidation products. *Fuel* **2022**, *318*, 123642. [[CrossRef](#)]
4. Deng, J.; Ma, X.; Zhang, Y.; Li, Y.; Zhu, W. Effects of pyrite on the spontaneous combustion of coal. *Int. J. Coal. Sci. Technol.* **2015**, *2*, 306–311. [[CrossRef](#)]
5. Liu, L.; Liu, Q.; Zhang, S.; Li, Y.; Yang, L. The thermal transformation behavior and products of pyrite during coal gangue combustion. *Fuel* **2022**, *324*, 124803. [[CrossRef](#)]
6. Ma, M.; Wang, W.; Zhang, K. Occurrence Characteristics of Fine-Grained Pyrite in Coal and Its Scaling Effect on Flotation Desulfurization. *ACS. Omega* **2022**, *7*, 42467–42481. [[CrossRef](#)]
7. Arisoy, A.; Beamish, B. Mutual effects of pyrite and moisture on coal self-heating rates and reaction rate data for pyrite oxidation. *Fuel* **2015**, *139*, 107–114. [[CrossRef](#)]
8. Dos Santos, E.C.; de Mendonça Silva, J.C.; Duarte, H.A. Pyrite Oxidation Mechanism by Oxygen in Aqueous Medium. *J. Phys. Chem. C* **2016**, *120*, 2760–2768. [[CrossRef](#)]
9. Feng-hua, Z.; Hong-fu, S.; Li, W.S. Migration of hazardous elements in acid coal mine drainage. *J. China Coal. Soc.* **2007**, *32*, 261–266.
10. Kiventerä, J.; Perumal, P.; Yliniemi, J.; Illikainen, M. Mine tailings as a raw material in alkali activation: A review. *Int. J. Miner. Metall. Mater.* **2020**, *27*, 1009–1020. [[CrossRef](#)]
11. Nesbitt, H.W.; Bancroft, G.M.; Pratt, A.R.; Scaini, M.J. Sulfur and iron surface states on fractured pyrite surfaces. *Am. Mineral.* **1998**, *83*, 1067–1076. [[CrossRef](#)]
12. Moses, C.O.; Nordstrom, D.K.; Herman, J.S.; Mills, A.L. Aqueous pyrite oxidation by dissolved oxygen and by ferric iron. *Geochim. Cosmochim. Acta* **1987**, *51*, 1561–1571. [[CrossRef](#)]
13. Yue, M.; Zhao, F.; Sun, H.F.; Ren, D.Y. The kinetics of oxidation reaction of pyrites from coal-bearing measure. *Mei T'an Hsueh Pao J. China Coal Soc.* **2005**, *30*, 75–79.
14. Mazumdar, A.; Goldberg, T.; Strauss, H. Abiotic oxidation of pyrite by Fe(III) in acidic media and its implications for sulfur isotope measurements of lattice-bound sulfate in sediments. *Chem. Geol.* **2008**, *253*, 30–37. [[CrossRef](#)]
15. Reedy, B.J.; Beattie, J.K.; Lowson, R.T. A vibrational spectroscopic ¹⁸O tracer study of pyrite oxidation. *Geochim. Cosmochim. Acta* **1991**, *55*, 1609–1614. [[CrossRef](#)]
16. Nicholson, R.V.; Gillham, R.W.; Reardon, E.J. Pyrite oxidation in carbonate-buffered solution: 2. Rate control by oxide coatings. *Geochim. Cosmochim. Acta* **1990**, *54*, 395–402. [[CrossRef](#)]
17. Boon, M.; Brassler, H.J.; Hansford, G.S.; Heijnen, J.J. Comparison of the oxidation kinetics of different pyrites in the presence of *Thiobacillus ferrooxidans* or *Leptospirillum ferrooxidans*. *Hydrometallurgy* **1999**, *53*, 57–72. [[CrossRef](#)]
18. Sun, H.; Chen, M.; Zou, L.; Shu, R.; Ruan, R. Study of the kinetics of pyrite oxidation under controlled redox potential. *Hydrometallurgy* **2015**, *155*, 13–19. [[CrossRef](#)]
19. Williams, K.P.; Kelly, D.P. Proposal for A New Class Within The Phylum Proteobacteria, Acidithiobacillia Classis Nov. with the Type Order Acidithiobacillales, and Emended Description of the Class Gammaproteobacteria. *Int. J. Syst. Evol. Microb.* **2013**, *63*, 2901–2906. [[CrossRef](#)] [[PubMed](#)]
20. Quatrini, R.; Appia-Ayme, C.; Denis, Y.; Ratouchniak, J.; Veloso, F.; Valdes, J.; Lefimil, C.; Silver, S.; Roberto, F.; Orellana, O.; et al. Insights into the iron and sulfur energetic metabolism of *Acidithiobacillus ferrooxidans* by microarray transcriptome profiling. *Hydrometallurgy* **2006**, *83*, 263–272. [[CrossRef](#)]

21. Sand, W.; Gehrke, T.; Jozsa, P.G.; Schippers, A. Direct versus indirect bioleaching. *Process Metall.* **1999**, *9*, 27–49.
22. Muhammad, S.N.; Kusin, F.M.; Madzin, Z. Coupled physicochemical and bacterial reduction mechanisms for passive remediation of sulfate- and metal-rich acid mine drainage. *Int. J. Environ. Sci. Technol.* **2018**, *15*, 2325–2336. [[CrossRef](#)]
23. Tu, B.; Wang, F.; Li, J.; Sha, J.; Lu, X.; Han, X. Analysis of Genes and Proteins in *Acidithiobacillus ferrooxidans* During Growth and Attachment on Pyrite Under Different Conditions. *Geomicrobiol. J.* **2013**, *30*, 255–267. [[CrossRef](#)]
24. Wang, C.; Bai, Z.; Xiao, Y.; Deng, J.; Shu, C. Effects of FeS₂ on the process of coal spontaneous combustion at low temperatures. *Process Saf. Environ.* **2020**, *142*, 165–173. [[CrossRef](#)]
25. Meng-hui, X.; Qin, Y.; Tong-sheng, Y.I. Sedimentary patterns and structural controls of late permian coal-bearing strata in Guizhou, China. *J. China Univ. Min. Technol.* **2006**, *35*, 778–782.
26. Xin, Z.D.; Jiang, B.; Qin, Y.; Zheng, Q.U.; Zhao, Y.; Yan, W.U. Pattern and mechanism of metamorphism of late permian coal in western Guizhou. *J. China Coal. Soc.* **2012**, *37*, 424–429.
27. Chen, H. *Geochemistry of the Ore-Forming Fluid of the Yaogangxian Tungsten Deposit in Southern Hunan, China*; Institute of Geochemistry Chinese Academy of Sciences: Guangzhou, China, 2008.
28. McKibben, M.A.; Barnes, H.L. Oxidation of pyrite in low temperature acidic solutions: Rate laws and surface textures. *Geochim. Cosmochim. Acta* **1986**, *50*, 1509–1520. [[CrossRef](#)]
29. Vöröš, D.; Geršlová, E.; Šimoníková, L.; Díaz-Somoano, M. Late Carboniferous palaeodepositional changes recorded by inorganic proxies and REE data from the coal-bearing strata: An example on the Czech part of the Upper Silesian Coal basin (USCB). *J. Nat. Gas. Sci. Eng.* **2022**, *107*, 104789. [[CrossRef](#)]
30. Qin, H.; Jia, J.; Lin, L.; Ni, H.; Wang, M.; Meng, L. Pyrite FeS₂ nanostructures: Synthesis, properties and applications. *Mater. Sci. Eng. B* **2018**, *236*, 104–124. [[CrossRef](#)]
31. Sun, J.; Bostick, B.C.; Mailloux, B.J.; Jamieson, J.; Yan, B.; Pitiranggon, M.; Chillrud, S.N. Arsenic mobilization from iron oxides in the presence of oxalic acid under hydrodynamic conditions. *Chemosphere* **2018**, *212*, 219–227. [[CrossRef](#)]
32. Rohwerder, T.; Sand, W. The sulfane sulfur of persulfides is the actual substrate of the sulfur-oxidizing enzymes from *Acidithiobacillus* and *Acidiphilium* spp. *Microbiology* **2003**, *149*, 1699–1710. [[CrossRef](#)] [[PubMed](#)]
33. Lilova, K.; Karamanev, D. Direct oxidation of copper sulfide by a biofilm of *Acidithiobacillus ferrooxidans*. *Hydrometallurgy* **2005**, *80*, 147–154. [[CrossRef](#)]
34. Zhu, T.; Lu, X.; Liu, H.; Li, J.; Zhu, X.; Lu, J.; Wang, R. Quantitative X-ray photoelectron spectroscopy-based depth profiling of bioleached arsenopyrite surface by *Acidithiobacillus ferrooxidans*. *Geochim. Cosmochim. Acta* **2014**, *127*, 120–139. [[CrossRef](#)]
35. Moon, H.S.; Kim, B.; Hyun, S.P.; Lee, Y.; Shin, D. Effect of the redox dynamics on microbial-mediated As transformation coupled with Fe and S in flow-through sediment columns. *J. Hazard Mater.* **2017**, *329*, 280–289. [[CrossRef](#)] [[PubMed](#)]
36. Li, J.; Lu, J.; Lu, X.; Tu, B.; Ouyang, B.; Han, X.; Wang, R. Sulfur Transformation in Microbially Mediated Pyrite Oxidation by *Acidithiobacillus ferrooxidans*: Insights from X-ray Photoelectron Spectroscopy-Based Quantitative Depth Profiling. *Geomicrobiol. J.* **2016**, *33*, 118–134. [[CrossRef](#)]
37. Lu, X.; Juan, L.I.; Huan, L.; WeiJie, L.I.; RuiYong, W.; Jianjun, L. Microbial oxidation of metal sulfides and its consequences. *Acta. Pet. Sin.* **2019**, *35*, 153–163.
38. Wenrui, J.; Zhihong, T.U.; Shu, Z.; Qi, W.U.; Zhi, D.; Huijun, H.E.; Chongmin, L.; Jie, L. A Brief Overview on the Mechanism and Kinetic Influencing Factors of the Pyrite Surface Oxidation. *Met. Mine* **2021**, *3*, 88–102.
39. Vera, M.; Schippers, A.; Sand, W. Progress in bioleaching: Fundamentals and mechanisms of bacterial metal sulfide oxidation—Part A. *Appl. Microbiol. Biot.* **2013**, *97*, 7529–7541. [[CrossRef](#)]
40. Tang, Y.; Ren, D.Y. The genesis of pyrites in coal. *Geol. Rev.* **1996**, *42*, 64–70.
41. Zhao, H.; Frimmel, H.E.; Jiang, S.; Dai, B. LA-ICP-MS trace element analysis of pyrite from the Xiaoqinling gold district, China: Implications for ore genesis. *Ore. Geol. Rev.* **2011**, *43*, 142–153. [[CrossRef](#)]
42. Belousov, I.; Large, R.R.; Meffre, S.; Danyushevsky, L.V.; Steadman, J.; Beardsmore, T. Pyrite compositions from VHMS and orogenic Au deposits in the Yilgarn Craton, Western Australia: Implications for gold and copper exploration. *Ore. Geol. Rev.* **2016**, *79*, 474–499. [[CrossRef](#)]
43. Zheng, Z.; Zheng, Y.; Tian, X.; Yang, Z.; Jiang, Y.; Zhao, F. Interactions between iron mineral-humic complexes and hexavalent chromium and the corresponding bio-effects. *Environ. Pollut.* **2018**, *241*, 265–271. [[CrossRef](#)] [[PubMed](#)]
44. Liu, Y.; Wu, S.; Liang, Z.; Liu, Y.; Ren, H.; Jia, S.; Han, X. Oxidation reactivity of As(III)-containing pyrites: Differences between structurally-incorporated and adsorbed As(III). *Chem. Geol.* **2019**, *522*, 223–239. [[CrossRef](#)]
45. Buckley, A.N.; Woods, R. The surface oxidation of pyrite. *Appl. Surf. Sci.* **1987**, *27*, 437–452. [[CrossRef](#)]
46. Loffredo, E.; Senesi, N. The Role of Natural Organic Matter (Humic Substances) on Adsorption of Pesticides Possessing Endocrine Disruptor Activity. *Nato Sci. Peace Secur. Ser. C Environ. Secur.* **2008**, 369–383.
47. Murphy, E.M.; Zachara, J.M. The role of sorbed humic substances on the distribution of organic and inorganic contaminants in groundwater. *Geoderma* **1995**, *67*, 103–124. [[CrossRef](#)]
48. Fubo, L.; Li, X.; Jun, L.; Qi, Z. Redox Behavior and Research Progress of Humic Acid. *Chem. Eur. J.* **2008**, *71*, 833–837.
49. Zheng, K.; Li, H.; Xu, L.; Li, S.; Wang, L.; Wen, X.; Liu, Q. The influence of humic acids on the weathering of pyrite: Electrochemical mechanism and environmental implications. *Environ. Pollut.* **2019**, *251*, 738–745. [[CrossRef](#)]
50. Yang, H.; Luo, W.; Gao, Y. Effect of *Acidithiobacillus ferrooxidans* on Humic-Acid Passivation Layer on Pyrite Surface. *Minerals* **2018**, *8*, 422. [[CrossRef](#)]

51. Zhang, L.; Li, Z.; Li, J.; Zhou, Y.; Yang, Y.; Tang, Y. Studies on the Low-Temp Oxidation of Coal Containing Organic Sulfur and the Corresponding Model Compounds. *Molecules* **2015**, *20*, 22241–22256. [[CrossRef](#)]
52. Kargi, F.; Robinson, J.M. Microbial oxidation of dibenzothiophene by the thermophilic organism *Sulfolobus acidocaldarius*. *Biotechnol. Bioeng.* **1984**, *26*, 687–690. [[CrossRef](#)] [[PubMed](#)]
53. Xue, Z.; Jun, C.J. Mechanism and Effect Factors for Spontaneous Combustion of Iron Sulfide in Natural Environment. *J. Combust. Sci. Technol.* **2007**, *5*, 443–447.
54. Nordstrom, D.; Alpers, C. Geochemistry of acid mine waters. In *The Environmental Geochemistry of Mineral Deposits, Part A: Processes, Techniques, and Health Issues*; Plumlee, G.S., Logsdon, M.J., Eds.; Society of Economic Geologists Inc.: Littleton, CO, USA, 1999; Volume 6A, pp. 133–156.
55. Wang, C.; Lv, C.; Bai, Z.; Deng, J.; Kang, F.; Xiao, Y.; Shu, C. Synergistic Acceleration Effect of Coal Spontaneous Combustion Caused By Moisture And Associated Pyrite. *Fuel* **2021**, *304*, 121458. [[CrossRef](#)]
56. Hu, Z.; Zhu, Q.; Xu, J.; Zhang, X. Effect of Bactericides on Control of Acidification Pollution and Spontaneous Combustion of Coal Gangue Dumps in China and Its Mechanism. *Sustainability* **2020**, *12*, 6697. [[CrossRef](#)]

Disclaimer/Publisher’s Note: The statements, opinions and data contained in all publications are solely those of the individual author(s) and contributor(s) and not of MDPI and/or the editor(s). MDPI and/or the editor(s) disclaim responsibility for any injury to people or property resulting from any ideas, methods, instructions or products referred to in the content.